THE JOURNAL OF PHYSICAL CHEMISTRY Letters

pubs.acs.org/JPCL Letter

Polarization of Valence Orbitals by the Intramolecular Electric Field from a Diffuse Dipole-Bound Electron

Dao-Fu Yuan,[†] Yuan Liu,[†] Chen-Hui Qian, G. Stephen Kocheril, Yue-Rou Zhang, Brenda M. Rubenstein, and Lai-Sheng Wang*

Cite This: *J. Phys. Chem. Lett.* 2020, 11, 7914–7919 Read Online

ACCESS | Metrics & More | Article Recommendations | Supporting Information

ABSTRACT: The diffuse electron in a dipole-bound state is spatially well separated from the valence electrons and is known to have negligible effects on the dipole-bound state's molecular structure. Here, we show that a dipole-bound state is observed in deprotonated 4-(2-phenylethynyl)-phenoxide anions, 348 cm^{-1} below the anion's detachment threshold. The photodetachment of the dipole-bound electron is observed to accompany a simultaneous shakeup process in valence orbitals in this aromatic molecular anion. This shakeup process is due to configuration mixing as a result of valence orbital polarization by the intramolecular electric field of the dipole-bound electron. This observation suggests that dipole-bound anions can serve as a new platform to probe how oriented electric fields influence the valence electronic structure of polyatomic molecules.

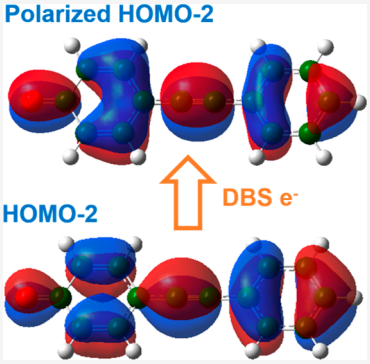

Because atoms and molecules are bound by electrostatic forces, their properties are expected to be influenced by external electric fields, such as in the Stark effect.[1] Recently, oriented external electric fields have been recognized as a "smart reagent" for catalyzing and controlling chemical reactions.[2−4] External electric fields can be generated from the tips of scanning tunneling microscopy[3] or within ultrashort laser pulses.[5−10] The intense electric fields in ultrashort laser pulses strongly distort the molecular electron density before inducing ionization or bond breaking in diatomic molecules.[5−7] Strong-field-induced orbital distortions are important for understanding the angular distributions of ionization yields.[8] In polyatomic molecules, distortions of valence molecular orbitals have been observed experimentally in strong laser fields before electron emission.[9,10]

Strong intramolecular electric fields (IEFs) exist in molecular systems, but they are usually treated as mean fields. Oriented IEFs caused by a single electron can be realized in dipole-bound states (DBSs), in which a diffuse electron is weakly bound by a molecular dipole far outside of the molecular cores, typically about 10 to 100 Å away.[11−14] Dipole-bound electrons have been shown to have very little effect on the structures of the molecular cores.[15,16] While electron correlation effects between the distant dipole-bound electron and the valence electrons of the neutral cores are known to be important for the accurate calculation of the binding energies of the dipole-bound electron,[13,17] how the oriented IEF of the dipole-bound electron influences the valence electrons has not been examined. Here, we show that the IEF exerted by a dipole-bound electron in an aromatic molecule, the deprotonated 4-(2-phenylethynyl)-phenoxide anion (PEP^-), can polarize the valence molecular orbitals of its neutral core and induce strong configuration mixing. A dipole-bound state is observed 348 cm^{-1} below the detachment threshold of PEP^- with three bound vibrational levels. Photodetachment of the dipole-bound electron from each of the bound vibrational levels of the DBS is observed to accompany a simultaneous valence excitation from HOMO−2 to the HOMO. This shakeup process is due to configuration mixing between the ground state of PEP and its second excited state, induced by the IEF produced by the dipole-bound electron. Thus, dipole-bound anions provide an exotic class of molecules, in which how IEFs influence the valence electronic structures of polyatomic molecules can be examined, analogous to the effects of strong laser fields.

A closed-shell neutral molecule with a sufficiently large dipole moment can bind an extra electron in a diffuse orbital.[11−13] Fermi and Teller first predicted a minimum dipole moment of 1.625 D for a finite dipole to bind an electron.[18] Accurate calculations of electron binding energies require *ab initio* methods that take into account electron correlation effects between the extra electron and the valence electrons.[13,14,17] Dipole-bound anions can be produced using

Received: August 17, 2020
Accepted: August 31, 2020
Published: September 8, 2020

https://dx.doi.org/10.1021/acs.jpclett.0c02514
J. Phys. Chem. Lett. 2020, 11, 7914–7919

Rydberg electron transfers[11,12] and have been investigated using field-induced detachment and photoelectron spectroscopy (PES).[19,20] Valence-bound anions may possess DBSs just below the detachment threshold, which were first observed using photodetachment spectroscopy by measuring their total detachment cross sections as a function of photon energy.[21−23] We have developed a high-resolution photoelectron imaging system coupled with a cryogenic ion trap (Figure S1 in the Supporting Information),[24] which has allowed the study of a wide range of anions from an electrospray ion source.[25,26] Photodetachment spectroscopy of cold anions has yielded vibrational information about the DBSs, which has been shown to be identical to that of their corresponding neutral cores.[15,16,25,26] Resonant PES can be performed by tuning the detachment laser to above-threshold vibrational resonances of the DBS and has been shown to yield much richer spectroscopic information than conventional nonresonant PES.[27]

Experimental details can be found in the Supporting Information.[24] Figure 1 displays the photoelectron images and spectra of PEP^- at two photon energies. The low-photon-energy spectrum (Figure 1b) yields an electron affinity (EA) of 2.6161 eV (21 100 cm^{-1}) for the neutral PEP radical, as defined by the 0_0^0 transition. Two peaks due to the excitations of low-frequency vibrations (1^1 and 1^12^1) are also observed. In the higher-photon-energy spectrum (Figure 1d), two electronically excited states of PEP are observed. Peaks X, A, and B represent electron detachment from the highest occupied molecular orbital (HOMO), HOMO−1, and HOMO−2 of PEP^-, respectively (Figure S2). The observed binding energies are given in Table S1. These assignments are supported by the good agreement between the simulated Franck−Condon factors and the observed vibrational progressions (Figure S3) as well as between the calculated and measured excitation energies (Table S1; see the Supporting Information for theoretical details). Furthermore, the photoelectron angular distributions in Figure 1c exhibit distinct (s + d) wave behavior for the three detachment channels, indicating that the parent orbitals are all of the π type, consistent with the nature of the valence MOs (Figure S2).

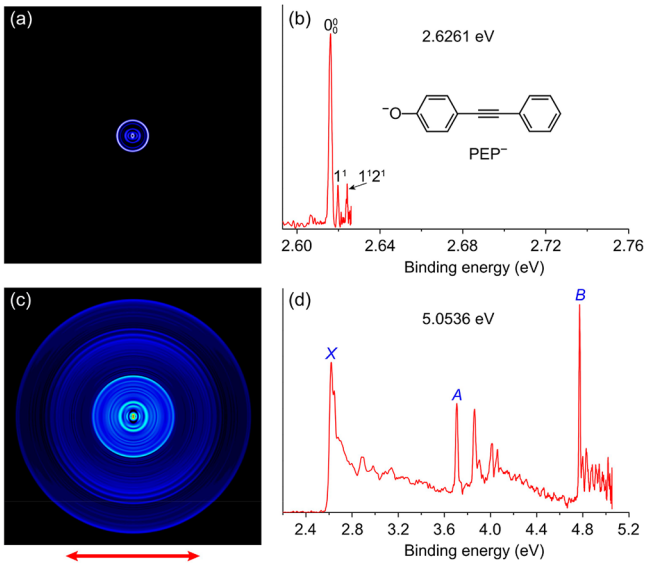

Figure 1. Photoelectron images and spectra of the PEP^- anion at 2.6261 eV (472.12 nm) and 5.0536 eV (245.34 nm). The double arrow below the image indicates the laser polarization direction. The peaks labeled as X, A, and B represent the 0−0 transition from the ground electronic state of PEP^- to the ground and the first two excited states of PEP, respectively.

Due to the large dipole moment (6.4 D) of the neutral PEP radical, a DBS is expected to exist below the detachment threshold of the PEP^- anion (Figure S4a). To search for the DBS, we scan the detachment laser around the threshold by monitoring the total photoelectron yield as a function of photon energy to obtain the photodetachment spectrum of PEP^- (Figure 2a). Indeed, many sharp resonance peaks

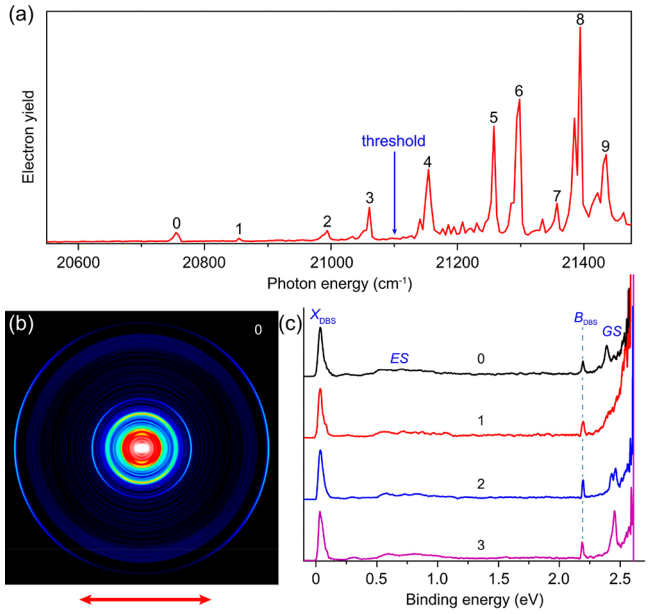

Figure 2. (a) Photodetachment spectrum. The blue arrow indicates the detachment threshold at 21 100 cm^{-1}. (b) R2PD photoelectron image mediated by the vibrational ground state of the DBS at 20 752 cm^{-1} (peak 0 in panel (a)). (c) R2PD photoelectron spectra mediated by the below-threshold vibrational states of the DBS at 20 752 cm^{-1} (peak 0), 20 854 cm^{-1} (peak 1), 20 991 cm^{-1} (peak 2), and 21 057 cm^{-1} (peak 3). The double arrow below the image indicates the laser polarization. The peaks labeled as X_{DBS} and B_{DBS} represent photoelectrons detached from the DBS, without and with the excitation of a valence electron, respectively. The signals labeled as GS and ES represent photoelectrons detached from the ground state and the first valence excited electronic state of PEP^-, respectively.

(labeled as 0−9 in Figure 2a) are observed in the photodetachment spectrum, corresponding to vibrational levels of the DBS. The weak peak at the lowest photon energy (peak 0) at 20 752 cm^{-1} (2.5729 eV) represents the ground vibrational level of the DBS, giving rise to a DBS binding energy of 348 cm^{-1} (below the detachment threshold of 21 100 cm^{-1}). Peaks 1−9 correspond to excited vibrational levels of the DBS. Below-threshold peaks 0−3 come from two-photon detachment processes, while above-threshold peaks 4−9, a.k.a. vibrational Feshbach resonances, are due to vibrational autodetachment. By tuning the detachment laser to the Feshbach resonances, we obtain six resonant photoelectron spectra (Figure S5), which are highly non-Franck−Condon in nature due to the $\Delta v = -1$ propensity rule for the vibrational autodetachment.[28,29] Specific vibrational levels are enhanced in the spectra shown in Figure S5 relative to the nonresonant

https://dx.doi.org/10.1021/acs.jpclett.0c02514
J. Phys. Chem. Lett. 2020, 11, 7914−7919

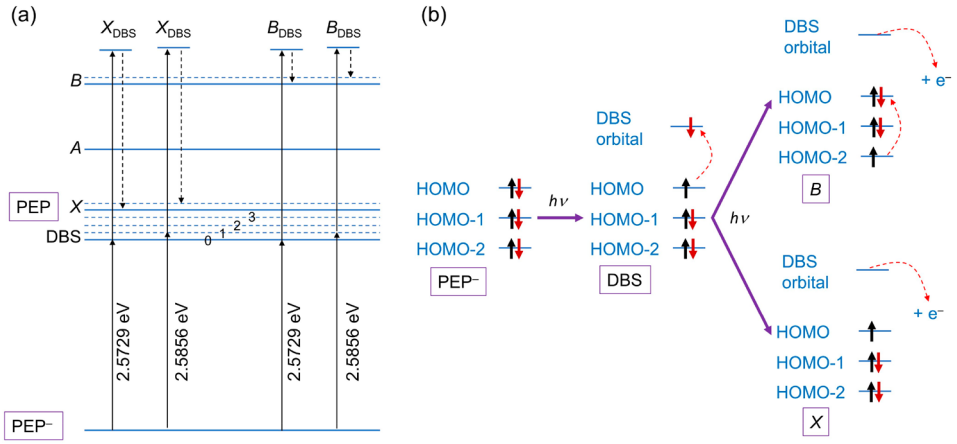

Figure 3. Schematics showing the adiabatic nature of the rR2PD and shakeup process. (a) Schematic energy-level diagram showing the excitations to two vibrational levels of the dipole-bound state at two photon energies (2.5729 and 2.5856 eV) and the adiabatic detachment process by the second photon. Two final states (X_{DBS} and B_{DBS}) are shown at each photon energy. (b) Schematics showing the electron configurations of the DBS upon absorption of the first photon and those following detachment of the dipole-bound electron by the second photon, which results in the ground state (X state) of PEP and its second excited state (B state) due to a shakeup process, i.e., the promotion of an electron from HOMO−2 to HOMO.

spectra.[27] Because the diffuse DBS electron has very little influence on the structures of the neutral cores, the DBS anions and the neutrals have been shown to have similar vibrational frequencies within our experimental uncertainty.[15,16,25−27] All of the 0−9 peaks observed in the photodetachment spectrum can be assigned to vibrational levels of the DBS (Table S2), according to the calculated neutral vibrational frequencies (Table S3) and the resonant photoelectron spectra (Figure S5). A complete energy-level diagram can be found in Figure S6, which summarizes the autodetachment processes.

The below-threshold vibrational levels (peaks 0−3 in Figure 2a) are observed due to resonant two-photon detachment (R2PD), where the first photon excites PEP^- to one of the below-threshold vibrational levels, followed by a second photon detaching the DBS electron. Figure 2c displays the four R2PD photoelectron spectra by measuring the electron kinetic energies when the detachment laser is tuned to the photon energies corresponding to peaks 0−3 in Figure 2a. The original photoelectron image at peak 0 is displayed in Figure 2b, and those images obtained at peaks 1−3 are given in Figure S7. Multiple features are observed, suggesting that different photoprocesses take place following the absorption of the first photon. The four photoelectron spectra share some similar features, even though they are taken at different photon energies. The lowest-binding-energy peak (labeled as X_{DBS} in Figure 2c) is from the expected R2PD process. The distinct p-wave angular distribution (Figure 2b and Figure S7) with an anisotropy parameter of 1.7 suggests that the dipole-bound electron resides in a σ-type orbital. The binding energies of the X_{DBS} peak in the four spectra are the same because of the adiabatic nature of the electron detachment from the DBS such that there is no change in vibrational energy from the DBS to the final neutral states, as depicted schematically in Figure 3a (left). The additional features in the higher-binding-energy region of the photoelectron spectra indicate other photodetachment processes. The broad and weak signals labeled as "ES" between 0.25 and 1.0 eV with a perpendicular angular distribution are assigned to detachment from a triplet valence excited state of PEP^- with a predicted binding energy of 0.8 eV. The population of the valence excited state is due to intersystem crossing from the DBS following the absorption of the first photon.[30] The diffuse and intense signals in the high-binding-energy region labeled as "GS" are due to detachment from the vibrational manifold of the ground electronic state of the PEP^- anion which is produced by an internal conversion process from the DBS,[27] followed by intramolecular vibrational energy redistribution.[31] The perpendicular angular distributions of these detachment features are similar to those in Figure 1c. These assignments are further confirmed by the excellent agreement between the experimental and theoretical anisotropy parameters of the detachment process (Figure S8).

The most surprising observation in the R2PD photoelectron spectra is the sharp peak labeled as "B_{DBS}" in the high-binding-energy region. The angular distribution of this peak has distinct p-wave character with an anisotropy parameter of 0.9, similar to that of the X_{DBS} peak. This peak cannot be due to detachment from an electronically excited state of the PEP^- anion like that for the ES feature because PEP^- does not possess such a low-lying excited state. The angular distribution of the B_{DBS} peak suggests that it comes from the direct detachment of the DBS electron, similar to the X_{DBS} peak. The energy separation between the B_{DBS} and X_{DBS} peaks is constant (2.16 eV), and their intensity ratios are similar ($I_{B_{DBS}}/I_{X_{DBS}} \approx 0.1$) in all four spectra (Figure 2c). The energy separation (2.16 eV) between the B_{DBS} and X_{DBS} peaks is identical to the separation between peak B and X (2.156 eV) in the nonresonant photoelectron spectrum (Figure 1d). Although it is energetically possible that the photoelectron signal is from the vibrational autodetachment of the DBS electron after the photon excites the valence electrons from the HOMO−2 to the vibrational levels of the HOMO, this process is ruled out because it will produce a nearly isotropic or (s + d)-wave angular distribution instead of the observed p-wave angular distribution. A more direct comparison between the R2PD photoelectron spectra and the single-photon nonresonant spectrum is given in Figure S9. Thus, all of the experimental evidence indicates that the B_{DBS} peak is due to a shakeup process, i.e., the detachment of the DBS electron accompanied by the simultaneous excitation of an electron from the HOMO−2 to the HOMO (Figure 3b). The constant binding energy of B_{DBS} is again due to the adiabatic nature of the

https://dx.doi.org/10.1021/acs.jpclett.0c02514
J. Phys. Chem. Lett. 2020, 11, 7914−7919

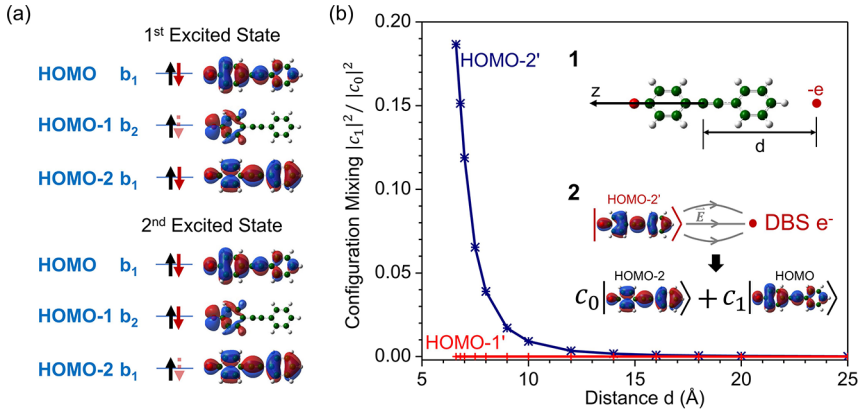

Figure 4. (a) Electronic configurations and orbital pictures of the first two neutral PEP excited states following the detachment of an electron from HOMO−1 (first excited state) and HOMO−2 (second excited state). The detachment spin-down electron is represented by a dashed arrow. The orbital pictures are plotted with an isovalue of 0.02. (b) Projection probabilities of the electric-field-polarized HOMO−1 (red +) and HOMO−2 (navy cross-dot) to the HOMO of neutral PEP as a function of the distance between the center of PEP and the dipole-bound electron approximated by a point charge in the calculation. Definition of distance d, with the point charge placed along the negative z axis (inset 1). The schematic of the oriented electric field polarizing HOMO−2 (upper row, in red ket), causing it to mix with the HOMO (lower row, inset 2). The mixing coefficients are plotted in the form of $|c_1|^2/|c_0|^2$. Only delocalized HOMO−2 has significant mixing with the HOMO, and the mixing increases dramatically as the point charge approaches the molecule.

detachment process, similar to that of the X_{DBS} peak, as schematically shown in Figure 3a (right). Both X_{DBS} and B_{DBS} peaks come from the detachment of the DBS electron with p-wave angular distributions, but their anisotropy is slightly different because the anisotropy parameter is kinetic-energy-dependent. The increase in the anisotropy parameter from 0.9 for peak B_{DBS} to 1.7 for peak X_{DBS} agrees well with the predicted monotonically increasing anisotropy parameter as a function of the photoelectron kinetic energies, when detachment occurs from a σ-type DBS orbital. (See the Supporting Information for details.)

Two-electron transitions or shakeup processes are well known in PES, which is among the most important techniques for probing electron correlation effects.[32] The current result is unprecedented and is completely unexpected because the highly diffuse DBS electron is known to have little effect on the neutral core. A recent study has shown that the dipole-bound electron is not even spin-coupled with the valence electrons in the neutral core in a DBS.[33] It is also surprising that the shakeup process is observed only from HOMO−2 to the HOMO, whereas the energetically more favorable channel from HOMO−1 to the HOMO, leading to the first excited state (A) at an excitation energy of 1.092 eV, is not observed in the R2PD photoelectron spectra in Figure 2c.

Further theoretical analyses have been performed to investigate the mechanisms of the shakeup process induced by the dipole-bound electron in PEP^-. We consider the first two energetically allowed valence excited states of neutral PEP, corresponding to the promotion of a spin-down electron from HOMO−1 and HOMO−2 to the singly occupied HOMO (Figure 4a), respectively. The observed shakeup peak (B_{DBS}) suggests that the dipole-bound electron strongly interacts with the electrons in HOMO−2 but not with those in HOMO−1. The strong interactions between the dipole-bound electrons and the HOMO−2 electrons induce a configuration mixing of the HOMO and HOMO−2. In other words, the orbital wave function of the spin-down electron ($\phi_{HOMO-2\downarrow'}$) in the DBS can be expressed as a linear combination of the HOMO and HOMO−2,

$$\phi_{HOMO-2\downarrow'} = c_0\phi_{HOMO-2\downarrow} + c_1\phi_{HOMO\downarrow} \quad (1)$$

where c_0 and c_1 are the mixing coefficients. The configuration mixing can be viewed as a result of the polarization of the valence electrons by the dipole-bound electron. Orbital mixing enabled by an external electric field is well known.[2,4,10] The delocalized nature of HOMO−2 (Figure 4a) means that it is more easily polarized by the oriented electric field exerted by the dipole-bound electron (inset 2 in Figure 4b) and that this polarization enables the mixing of HOMO−2 with the HOMO. The orientation of the electric field from the dipole-bound electron is determined by the direction of the dipole moment of neutral PEP, which lies along the molecular z axis with the largest polarizability α_{zz} (Table S4 and Figure S10). On the other hand, more localized HOMO−1 is expected to be less polarized by the dipole-bound electron.

The relative intensities of the observed X_{DBS} and B_{DBS} peaks in the photoelectron spectra (Figure 2c) can then be related to mixing coefficients c_0 and c_1, respectively. The intensities of peaks X_{DBS} and B_{DBS} can be expressed as the absolute square of the electric-dipole transition amplitude M_k from the DBS of PEP^- to the neutral PEP plus a free electron with linear momentum $\mathbf{k}$

$$\mathbf{M_k} = C\langle\Psi^{\mathbf{k}}_{val}(\mathbf{r_1}, \mathbf{r_2}, \cdots, \mathbf{r_N})\phi_{\mathbf{k}}(\mathbf{r_{N+1}}) |\varepsilon\cdot(\boldsymbol{\mu}_{val} + \boldsymbol{\mu}_{DBS})|\Psi'_{val}(\mathbf{r_1}, \mathbf{r_2}, \cdots, \mathbf{r_N})\phi_{DBS}(\mathbf{r_{N+1}})\rangle \quad (2)$$

where $\boldsymbol{\mu}_{val} = e\sum_{i=1}^{N}\mathbf{r_i}$ and $\boldsymbol{\mu}_{DBS} = e\mathbf{r_{N+1}}$ are the dipole operators for the valence electrons and the DBS electron; ϕ_{DBS} and Ψ'_{val} are the wave functions of the dipole-bound electrons and the neutral core in the DBS; and $\phi_{\mathbf{k}}$ and $\Psi^{\mathbf{k}}_{val}$ are the wave functions of the detached electron in the continuum with momentum $\mathbf{k}$ and the neutral core upon electron detachment, respectively. Vectors $\mathbf{r_1}$, $\mathbf{r_2}$,⋯, $\mathbf{r_N}$ stand for the coordinates of the N valence electrons in neutral PEP, $\mathbf{r_{N+1}}$ represents the coordinates of the dipole-bound electron, and C is a constant. We write the total wave function as a product of the valence part and DBS part because they are spatially well separated with a negligible overlap. Equation 2 can be used to

https://dx.doi.org/10.1021/acs.jpclett.0c02514
J. Phys. Chem. Lett. 2020, 11, 7914−7919

derive a relative intensity ratio between peaks B_{DBS} and X_{DBS} (Supporting Information)

$$I_{B_{DBS}}/I_{X_{DBS}} = F_{\mathbf{k_0},\mathbf{k_1}}{}^{*}|c_1|^2/|c_0|^2 \quad (3)$$

where $F_{\mathbf{k_0},\mathbf{k_1}}$ denotes the ratio between the dipole-transition probability of the DBS electron to the continuum with two different momenta $\mathbf{k_0}$ (for the X_{DBS} peak) and $\mathbf{k_1}$ (for the B_{DBS} peak).

To evaluate the configuration mixing induced by the dipole-bound electron, we consider the molecular orbitals of neutral PEP in the presence of a negative point charge positioned along the z axis at a distance from the PEP molecule to approximate the electric field induced by the dipole-bound electron (inset 1 Figure 4b) and then project it onto $\phi_{HOMO\downarrow}$. The resulting $|c_1|^2/|c_0|^2$ ratios for HOMO−1′ and HOMO−2′ are plotted in Figure 4b. Note that there is no configuration mixing without the point charge (distance → ∝). As the point charge is closer to the PEP molecule, namely, as the oriented electric field becomes stronger, the contribution of the HOMO to HOMO−2′ increases rapidly and $|c_1|^2/|c_0|^2$ reaches about 4% when the distance between the electron and the center of the PEP is about 8 Å. (The electric field near the molecular center produced by the point charge is about 0.0044 au.[34]) On the other hand, the mixing coefficient of HOMO−1 with the HOMO remains zero, independent of the presence of the point charge. Since $F_{\mathbf{k_0},\mathbf{k_1}}$ is a constant that is close to 1 (see the Supporting Information for details), the theoretical estimate agrees qualitatively with the observed B_{DBS}/X_{DBS} peak ratio of ∼10%. In the presence of the oriented electric field from the dipole-bound electron approximated by the point charge, we observe a significant change in the shape of HOMO−2′ in the DBS compared to HOMO−2 of neutral PEP (inset 2 in Figure 4b and Figure S10). We also find that the magnitude and direction of the electric field are important to the degree of valence orbital deformation and configuration mixing. These anisotropic effects in the orbital polarization are shown in Figure S10, where the molecular orbitals and mixing coefficient c_1 for HOMO−1 or HOMO−2 with the HOMO, when polarized by an electric field along different directions, are shown. Clearly, HOMO−2 exhibits the largest mixing with the HOMO when polarized along the molecular axis (dipole direction), providing direct evidence of the role that the DBS electron plays in configuration mixing. The delocalized nature of HOMO−2 in PEP makes it particularly susceptible to the polarization effect of the diffuse dipole-bound electron.[34]

The orbital deformation by the intramolecular electric field from the diffuse dipole-bound electron is similar to that induced by an external field, such as in an ultrafast intense laser pulse.[9,10] The IEFs created by such dipole-bound electrons can be tuned by the magnitude of the molecular dipole or its orientation by modifying the molecular structures. Delocalized molecular orbitals that are more sensitive to IEFs are prevalent in all aromatic hydrocarbon compounds. This class of molecules provides ideal systems for investigating how oriented IEFs influence valence electronic structures complementary to those in ultrafast laser pulses[9,10] or other types of external electric fields.[2−4]

■ ASSOCIATED CONTENT

Supporting Information

The Supporting Information is available free of charge at https://pubs.acs.org/doi/10.1021/acs.jpclett.0c02514.

Experimental and theoretical methods and additional results (PDF)

■ AUTHOR INFORMATION

Corresponding Author

Lai-Sheng Wang − *Department of Chemistry, Brown University, Providence, Rhode Island 02912, United States;* orcid.org/0000-0003-1816-5738; Email: Lai-Sheng_Wang@brown.edu

Authors

Dao-Fu Yuan − *Department of Chemistry, Brown University, Providence, Rhode Island 02912, United States;* orcid.org/0000-0001-8461-6889

Yuan Liu − *Department of Chemistry, Brown University, Providence, Rhode Island 02912, United States;* orcid.org/0000-0003-1468-942X

Chen-Hui Qian − *Department of Chemistry, Brown University, Providence, Rhode Island 02912, United States*

G. Stephen Kocheril − *Department of Chemistry, Brown University, Providence, Rhode Island 02912, United States;* orcid.org/0000-0003-1388-6472

Yue-Rou Zhang − *Department of Chemistry, Brown University, Providence, Rhode Island 02912, United States*

Brenda M. Rubenstein − *Department of Chemistry, Brown University, Providence, Rhode Island 02912, United States*

Complete contact information is available at: https://pubs.acs.org/10.1021/acs.jpclett.0c02514

Author Contributions

†D.-F.Y and Y.L. contributed equally to this work.

Notes

The authors declare no competing financial interest.

■ ACKNOWLEDGMENTS

This work was supported by the U.S. Department of Energy, Office of Basic Energy Sciences, Chemical Sciences, Geosciences, and Biosciences Division under grant DESC0018679. Y.L. thanks Prof. Chuan-Gang Ning from Tsinghua University for providing part of the computer codes on the anisotropy parameter calculation. The calculations are performed using resources from the Center for Computation and Visualization of Brown University. Y.L. was supported by the Open Graduate Education program of Brown University.

■ REFERENCES

(1) Stark, J. Observation of the Separation of Spectral Lines by an Electric Field. *Nature* **1913**, *92*, 401−401.

(2) Shaik, S.; Mandal, D.; Ramanan, R. Oriented Electric Fields as Future Smart Reagents in Chemistry. *Nat. Chem.* **2016**, *8*, 1091−1098.

(3) Aragonés, A.; Haworth, N. L.; Darwish, N.; Ciampi, S.; Bloomfield, N. J.; Wallace, G. G.; Diez-Perez, I.; Coote, M. L. Electrostatic Catalysis of a Diels-Alder Reaction. *Nature* **2016**, *531*, 88−91.

(4) Shaik, S.; Ramanan, R.; Danovich, D.; Mandal, D. Structure and Reactivity/Selectivity Control by Oriented-External Electric Fields. *Chem. Soc. Rev.* **2018**, *47*, 5125−5145.

(5) Kling, M. F.; Siedschlag, Ch.; Verhoef, A. J.; Khan, J. I.; Scultze, M.; Uphues, Th.; Ni, Y.; Uiberacker, M.; Drescher, M.; Krausz, F.; Vrakking, M. J. J. Control of Electron Localization in Molecular Dissociation. *Science* **2006**, *312*, 246−248.

(6) Meckel, M.; Comtois, D.; Zeidler, D.; Staudte, A.; Pavicic, D.; Bandulet, H. C.; Pepin, H.; Kieffer, J. C.; Dorner, R.; Villeneuve, D.

M.; Corkum, P. B. Laser-Induced Electron Tunneling and Diffraction. *Science* **2008**, *320*, 1478−1482.
(7) Akagi, H.; Otobe, T.; Staudte, A.; Shiner, A.; Turner, F.; Dorner, R.; Villeneuve, D. M.; Corkum, P. B. Laser Tunnel Ionization from Multiple Orbitals in HCl. *Science* **2009**, *325*, 1364−1367.
(8) Spiewanowski, M. D.; Madsen, L. B. Alignment- and Orientation-Dependent Strong-Field Ionization of Molecules: Field-Induced Orbital Distortion Effects. *Phys. Rev. A: At., Mol., Opt. Phys.* **2015**, *91*, 043406.
(9) Kraus, P. M.; Tolstikhin, O. I.; Baykusheva, D.; Rupenyan, A.; Schneider, J.; Bisgaard, C. Z.; Morishita, T.; Jensen, F.; Madsen, L. B.; Worner, H. J. Observation of Laser-Induced Electronic Structure in Oriented Polyatomic Molecules. *Nat. Commun.* **2015**, *6*, 7039.
(10) Akagi, H.; Otobe, T.; Itakura, R. Deformation of an Inner Valence Molecular Orbital in Ethanol by an Intense Laser Field. *Sci. Adv.* **2019**, *5*, No. eaaw1885.
(11) Desfrancois, C.; Abdoul-Carime, H.; Schermann, J. P. Ground-State Dipole-Bound Anions. *Int. J. Mod. Phys. B* **1996**, *10*, 1339−1395.
(12) Compton, R. N.; Hammer, N. I. Multiple-Bound Molecular Anions. *Adv. Gas Phase Ion Chem.* **2001**, *4*, 257−305.
(13) Jordan, K. D.; Wang, F. Theory of Dipole-Bound Anions. *Annu. Rev. Phys. Chem.* **2003**, *54*, 367−396.
(14) Simons, J. Molecular Anions. *J. Phys. Chem. A* **2008**, *112*, 6401−6511.
(15) Liu, H. T.; Ning, C. G.; Huang, D. L.; Dau, P. D.; Wang, L. S. Observation of Mode-Specific Vibrational Autodetachment from Dipole-Bound States of Cold Anions. *Angew. Chem. Angew. Chem., Int. Ed.* **2013**, *52*, 8976−8979.
(16) Liu, H. T.; Ning, C. G.; Huang, D. L.; Wang, L. S. Vibrational Spectroscopy of the Dehydrogenated Uracil Radical via Autodetachment of Dipole-Bound Excited States of Cold Anions. *Angew. Chem., Int. Ed.* **2014**, *53*, 2464−2468.
(17) Gutowski, M.; Skurski, P.; Boldyrev, A.; Simons, J.; Jordan, K. D. The Contribution of Electron Correlation to the Stability of Dipole-Bound Anionic States. *Phys. Rev. A: At., Mol., Opt. Phys.* **1996**, *54*, 1906−1909.
(18) Fermi, E.; Teller, E. The Capture of Negative Mesotrons in Matter. *Phys. Rev.* **1947**, *72*, 399−408.
(19) Desfrancois, C.; Baillon, B.; Schermann, J. P.; Arnold, S. T.; Hendricks, J. H.; Bowen, K. H. Prediction and Observation of a New, Ground State, Dipole-Bound Dimer Anion: the Mixed Water/Ammonia System. *Phys. Rev. Lett.* **1994**, *72*, 48−51.
(20) Ciborowski, S. M.; Liu, G.; Graham, J. D.; Buytendyk, A. M.; Bowen, K. H. Dipole-Bound Anions: Formed by Rydberg Electron Transfer (RET) and Studied by Velocity Map Imaging-Anion Photoelectron Spectroscopy (VMI-aPES). *Eur. Phys. J. D* **2018**, *72*, 139.
(21) Jackson, R. L.; Zimmerman, A. H.; Brauman, J. I. Resonant States at Threshold Observed in Electron Photodetachment Cross Sections of Polyatomic Negative Ions. *J. Chem. Phys.* **1979**, *71*, 2088−2094.
(22) Lykke, K. R.; Mead, R. D.; Lineberger, W. C. Observation of Dipole-Bound States of Negative Ions. *Phys. Rev. Lett.* **1984**, *52*, 2221−2224.
(23) Marks, J.; Brauman, J. I.; Mead, R. D.; Lykke, K. R.; Lineberger, W. C. Spectroscopy and Dynamics of the Dipole-Supported State of Acetyl Fluoride Enolate Anion. *J. Chem. Phys.* **1988**, *88*, 6785−6792.
(24) Wang, L. S. Electrospray Photoelectron Spectroscopy: from Multiply-Charged Anions to Ultracold Anions. *J. Chem. Phys.* **2015**, *143*, 040901.
(25) Huang, D. L.; Ning, C. G.; Liu, H. T.; Wang, L. S. Conformation-Selective Resonant Photoelectron Spectroscopy via Dipole-Bound States of Cold Anions. *J. Phys. Chem. Lett.* **2015**, *6*, 2153−2157.
(26) Zhu, G. Z.; Qian, C. H.; Wang, L. S. Tautomer-Specific Resonant Photoelectron Imaging of Deprotonated Cytosine Anions. *Angew. Chem., Int. Ed.* **2019**, *58*, 7856−7860.
(27) Zhu, G. Z.; Wang, L. S. High-Resolution Photoelectron Imaging and Resonant Photoelectron Spectroscopy via Noncovalent-Bound Excited States of Cryogenically-Cooled Anions. *Chem. Sci.* **2019**, *10*, 9409−9423.
(28) Berry, R. S. Ionization of Molecules at Low Energies. *J. Chem. Phys.* **1966**, *45*, 1228−1245.
(29) Simons, J. Propensity Rules for Vibrational-Induced Electron Detachment of Anions. *J. Am. Chem. Soc.* **1981**, *103*, 3971−3976.
(30) Zhu, G. Z.; Cheung, L. F.; Liu, Y.; Qian, C. H.; Wang, L. S. Resonant Two-Photon Photoelectron Imaging and Intersystem Crossing from Excited Dipole-Bound States of Cold Anions. *J. Phys. Chem. Lett.* **2019**, *10*, 4339−4344.
(31) Freed, K. F.; Nitzan, A. Intramolecular Vibrational Energy Redistribution and the Time Evolution of Molecular Fluorescence. *J. Chem. Phys.* **1980**, *73*, 4765−4778.
(32) Heimann, P. A.; Becker, U.; Kerkhoff, H. G.; Langer, B.; Szostak, D.; Wehlitz, R.; Lindle, D. W.; Ferrett, T. A.; Shirley, D. A. Helium and Neon Photoelectron Satellites at Threshold. *Phys. Rev. A: At., Mol., Opt. Phys.* **1986**, *34*, 3782−3791.
(33) Czekner, J.; Cheung, L. F.; Kocheril, G. S.; Wang, L. S. Probing the Coupling of a Dipole-Bound Electron with the Molecular Core. *Chem. Sci.* **2019**, *10*, 1386−1391.
(34) The weighted center of the DBS orbital wave function (Figure S4a) is calculated to be ∼8.8 Å from the center of PEP. The electric field at the center of PEP is integrated to be about 0.0019 au using the DBS orbital wave function. This field strength is about a factor of 10 weaker than that in a typical ultrashort laser pulse. However, the large polarizability of the delocalized electrons in aromatic molecules makes them more sensitive to the intramolecular electric field exerted by the diffuse dipole-bound electron.

https://dx.doi.org/10.1021/acs.jpclett.0c02514
J. Phys. Chem. Lett. 2020, 11, 7914−7919